

InAlAs EPITAXIAL GROWTH FOR WIDE BAND GAP SOLAR CELLS

Marina S. Leite¹, Robyn L. Woo², William D. Hong², Daniel C. Law², and Harry A. Atwater¹

¹Thomas J. Watson Laboratories of Applied Physics, California Institute of Technology, Pasadena, CA 91125

²Boeing-Spectrolab Inc., 12500 Gladstone Avenue, Sylmar, CA 91342

ABSTRACT

We demonstrate high quality InAlAs epitaxial growth by metalorganic vapor phase epitaxy and wide band gap solar cell fabrication. X-ray diffraction and transmission electron microscopy were used to characterize the crystalline quality of the epitaxial InAlAs grown. InAlAs solar cells lattice-matched to InP were grown and electrically characterized under AM 1.5 global 1-sun illumination. Window layers with different composition and, therefore, band gap energies were used to compare its effect on the overall device performance. In order to improve the electrical contact at the top window (Al-rich), an InGaAs cap layer was used. The resulting first generation of InAlAs solar cells showed an efficiency higher than 14 %, open circuit voltage of $V_{oc} = 1$ V, $J_{sc} = 19.3$ mA/cm², and maximum external quantum efficiency of 81 %.

INTRODUCTION

From all the currently available technologies for photovoltaics, III-V semiconductor alloyed materials are the only option for achieving high efficiency single and multijunction solar cells. For instance, thin film GaAs single junction solar cell can achieve efficiencies over 27 % under global AM 1.5 spectrum (1 kW/m²) [1]. For multijunction configurations, terrestrial concentrator cells made of metamorphic InGaP/GaAs/InGaAs can achieve > 41 % by using metamorphic epitaxial growth [1,2].

Direct band gap III-V semiconductor alloys offer the advantage of effectively converting sunlight to electricity by using a small amount of material, either by substrate reuse or by using a reduced area, which drives its cost down. However, one of the biggest challenges to achieve a high efficiency multijunction solar cell is to match the current between the different subcells in order to maximize light collection over the solar spectrum [3]. The conventional approach for multijunction designs uses the GaAs-GaInP alloy materials system. An interesting and alternative option that allows for good current matching between different subcells is the InAlAs/InGaAsP system, using a combination of InAlAs/InGaAsP/InGaAs subcells, lattice-matched to InP (see solid grey squares in Fig. 1). A high efficiency top InAlAs wide band gap subcell is crucial for accessing short wavelengths (~ 0.4 – 0.6 μm). Additionally, the successful growth of wide band gap cells,

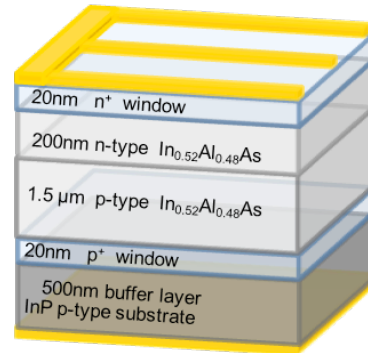
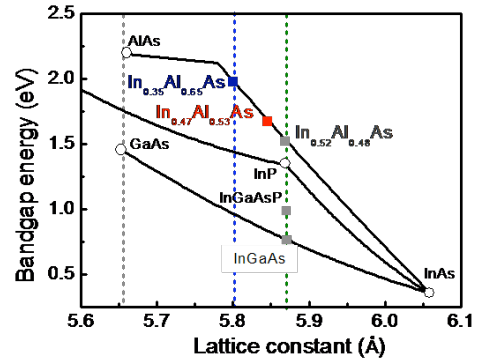


Figure 1: (Top) Band gap energy vs. lattice constant diagram for selected III-V semiconductor alloys. The black solid lines refer to the ternary alloys formed by combining different III-V elements; the dashed lines indicate the lattice constant used on the conventional GaAs-based approach (grey) and an alternative InP-based design (green). The blue dashed line corresponds to an optimized three and four junction design. Open circles refer to substrates, gray solid squares refer to the subcells lattice-matched to InP, red and blue solid squares correspond to the band gap energy E_g of the different window layers used in the fabricated InAlAs solar cells. Bottom: Schematic of the InAlAs solar cell grown by metalorganic vapor phase epitaxy. The window layers are $In_xAl_{1-x}As$ alloys with different compositions ($x = 0.47$ and 0.35). Yellow refers to the top and bottom contact layers.

coupled with a 5.80 Å substrate, as pointed out by the dashed blue line in Fig. 1, can enable an ideal set of 3 and 4 junction solar cells with selected band gaps.

InAlAs CRYSTAL CHARACTERIZATION

For high device efficiency, the first step is the synthesis of high quality crystalline $\text{In}_{0.52}\text{Al}_{0.48}\text{As}$, lattice-matched to InP. Fig. 1 shows a schematic of the InAlAs solar cell grown on 2-inch InP substrates, using a Veeco E400 metalorganic vapor phase epitaxy reactor operated at low pressure. Several 1.0 cm^2 cells were produced. The p - n absorber layer is formed by $\text{In}_{0.52}\text{Al}_{0.48}\text{As}$, which is lattice-matched to the substrate. In order to understand the role of the window layer in reducing the surface recombination velocity and how it affects the cell's overall performance, $\text{In}_x\text{Al}_{1-x}\text{As}$ alloys of different compositions were grown for comparison. The window layers have In fraction (x) equal to 0.47 (cell I) and 0.35 (cell II), corresponding to lattice constants of 5.847 \AA and 5.800 \AA , and tensile strain values of $+0.37 \%$ and $+1.17 \%$, respectively.

To confirm that the window layers are coherently-strained and free of dislocations with respect to the p - n absorber layer, X-ray diffraction (XRD) measurements were performed using grazing incidence geometry. Fig. 2(a) and (b) show the XRD ω - 2θ measurements at (0 0 4) reflection for solar cells I and II (inset of figures show each cell structure). In both cases, the 20 nm thick top window layer is coherently-strained with respect to the p - n absorber layer. The p - n absorber layers peak diffract at the same Bragg condition as the InP substrate. The width and position of the broad window peaks are in agreement with simulations of equivalent structures, as shown on the inset of Fig. 2. Although the cells have a high content of Al, epitaxial material was successfully grown.

Cross-section Transmission Electron Microscopy (TEM) measurements were performed to corroborate the XRD results. Figure 3(a) shows the cross-section of solar cell II. The electron diffraction pattern of the solar cell active region [see Fig. 3(b)] shows well-defined spots at the InP zone axis, characteristic of a high quality epitaxial crystal. Figure 3(c) shows an atomic resolution TEM image of the interface between the InP buffer layer, the 20 nm $\text{In}_{0.47}\text{Al}_{0.53}\text{As}$ window layer in solar cell I and the p - n $\text{In}_{0.52}\text{Al}_{0.48}\text{As}$ absorber layer. The yellow arrows indicate the interfaces between the different layers, which are very smooth, as desired—no dislocations were found.

The optical properties of the InAlAs alloy were characterized by time-resolved room temperature photoluminescence measurements. Lifetimes equal to 195 and 215 ps were measured for alloyed layers with composition similar to solar cells I and II, respectively (Fig. 4). Hall mobility measurements were performed on a 930 nm thick $\text{In}_{0.52}\text{Al}_{0.48}\text{As}$ n -doped layer with $N_d = 2.68 \times 10^{18} \text{ cm}^{-3}$ carrier density, and the mobility was equal $667 \text{ cm}^2/\text{V}\cdot\text{s}$. Therefore, a lower bound on the minority carrier diffusion length in the $\text{In}_{0.52}\text{Al}_{0.48}\text{As}$ alloy grown of approximately $1.0 \mu\text{m}$ was obtained.

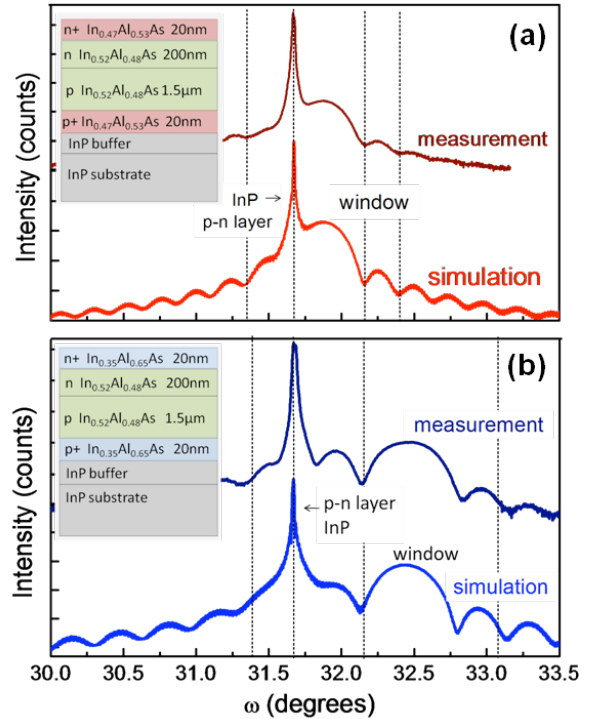


Figure 2: X-ray diffraction ω - 2θ measurement and simulation of (a) solar cell I, with 20 nm $\text{In}_{0.47}\text{Al}_{0.53}\text{As}$ window layer, corresponding to $+0.37 \%$ strain, and (b) solar cell II, with 20 nm $\text{In}_{0.47}\text{Al}_{0.53}\text{As}$ window layer, corresponding to $+1.17 \%$ strain. The simulations of the same structures, with same strain values, confirm that the heterostructures are dislocation-free. Inset: solar cell structures. Measurements settings: (0 0 4) reflection, $\lambda = 1.54056 \text{ \AA}$, 40 mA , receiving slit: $1/2^\circ$.

The high Al content of the window layers is important to reduce surface recombination velocity within the solar cells. By using a crystalline semiconductor compound with a band gap higher than the p - n absorber layer ($> 1.47 \text{ eV}$) one can also minimize the parasitic light absorption from the window layer. However, the $\text{In}_x\text{Al}_{1-x}\text{As}$ alloys used as window layers prevent the use of an anti-reflection (AR) coating containing oxygen. The high Al content alloys used for the window layers ($x = 0.47$ and 0.65) oxidize immediately, destroying the device. Therefore, a 20 nm thick InGaAs cap layer with the same lattice constant as the p - n absorber layer was used in order to passivate the surface of solar cell II and allow for incorporating an optimized AR coating (solar cell III) [4,5].

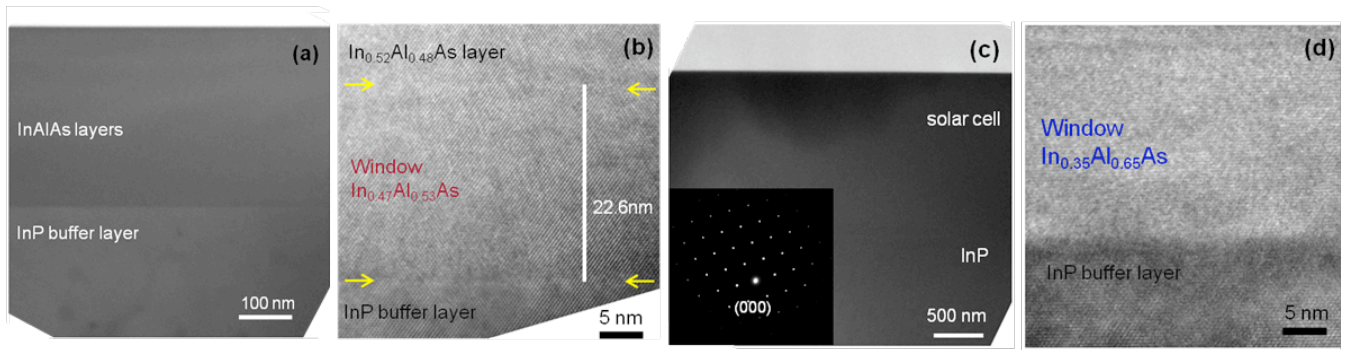


Figure 3: (a) Cross-section Transmission Electron Microscopy (TEM) image of solar cell I showing the interface between the InP buffer layer and the $\text{In}_x\text{Al}_{1-x}\text{As}$ active layers. (b) Atomic resolution image showing the dislocation-free interface between $\text{In}_x\text{Al}_{1-x}\text{As}$ alloys with different compositions. (c) TEM of solar cell II with $1.7\ \mu\text{m}$ in thickness. Inset: Electron diffraction pattern of the solar cell. Note the well-defined spots in the pattern, which are characteristic of an epitaxial crystal (InP zone axis). (d) High resolution cross-section TEM image of the interfaces between the InP buffer layer, 20 nm $\text{In}_{0.35}\text{Al}_{0.65}\text{As}$ window layer, and the p - n $\text{In}_{0.47}\text{Al}_{0.53}\text{As}$ absorber layer for solar cell II.

SOLAR CELL CHARACTERIZATION

Electrical measurements were performed under AM 1.5 global 1-sun illumination ($100\ \text{mW}/\text{cm}^2$) in order to compare the devices' performance. Fig. 5 shows light J-V curves and external quantum efficiency measurements for representative cells. As shown in Fig. 5(a), solar cell I (red data) has an open circuit voltage (V_{oc}) equal to 756 mV, a short circuit current (J_{sc}) of $9.3\ \text{mA}/\text{cm}^2$, and Fill Factor (FF) of 54 % resulting in an efficiency (η) equal to 4.6 %. The performance of the InAlAs solar cell is slightly improved by using the higher band gap window layer (1.98 eV) – see J-V curve for solar cell II with higher V_{oc} (767 mV) and J_{sc} ($11.7\ \text{mA}/\text{cm}^2$), as a direct consequence of less parasitic light absorption by the top window layer.

By adding the InGaAs cap layer and an optimized AR coating (solar cell III) the performance of the cell improves significantly. As shown in Fig. 5(a), both V_{oc} and J_{sc} increased dramatically ($990\ \text{mV}$ and $19.3\ \text{mA}/\text{cm}^2$, respectively), leading to an efficiency equal to 14.2 ± 1.0 %. Additionally, to allow for the use of an AR coating, the InGaAs improves the electrical contact of the cell, which is confirmed by a better FF (74 %). The V_{oc} of solar cell III is very close to the maximum value expected for a direct band gap material with $E_g = 1.47\ \text{eV}$. Several solar cells with $1.0\ \text{cm}^2$ in active area were characterized, and the table in Fig. 5 summarizes all figures of merit for cells I, II, and III.

The external quantum efficiency (EQE) measurements of the solar cells were performed under chopped monochromatic illumination at 30 Hz, using lock-in detection to record the photocurrent from each solar cell as a function of wavelength. Solar cells I and II showed a maximum EQE equal to 38 and 44 %, respectively. The EQE of solar cell III improved by approximately 5 % in the blue region of the spectrum and was enhanced by over 50 % in the visible and near IR, compared to solar cell II, achieving a maximum value of 81 % at 765 nm.

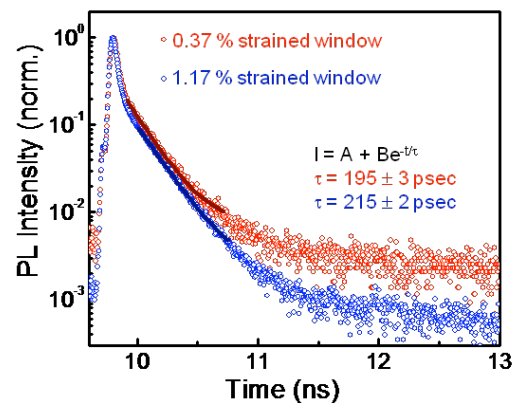
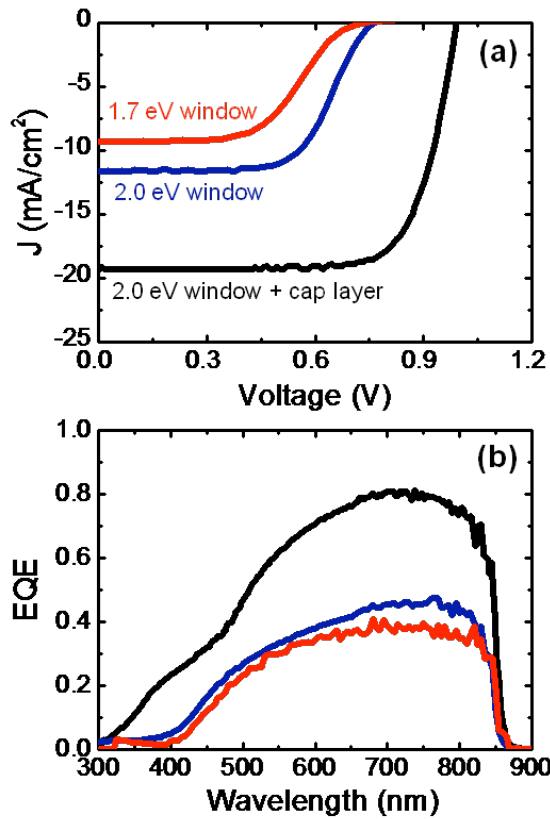


Figure 4: Room temperature time-resolved photoluminescence measurements for heterostructures with top layers similar to solar cell I (red) and solar cell II (blue). The solid lines show the exponential fit for both decays.

CONCLUSION

In conclusion, by controlling defects such as dislocations in $\text{In}_x\text{Al}_{1-x}\text{As}$ layers with different compositions, we fabricated wide band gap InAlAs solar cells. XRD and TEM confirmed that the material grown by metalorganic vapor deposition is dislocation-free, leading to an epitaxial crystal with promising optical properties. The InAlAs p - n absorber layer was lattice-matched to the InP substrate, and a top wide band gap $\text{In}_{0.35}\text{Al}_{0.65}\text{As}$ window layer was used to prevent surface recombination and allow more light absorption within the absorber layer. The InAlAs fabricated solar cell showed an efficiency of 14.2 % and an EQE of up to 81 %. The demonstration of an InAlAs wide band gap solar cell presented here opens up the possibility for an innovative multijunction solar cell design based on InP lattice-matched alloys.



	V_{oc} (mV)	J_{sc} (mA/cm ²)	FF (%)	η (%)
Cell I	756 ± 50	9.3 ± 2.5	54 ± 5	4.6 ± 0.8
Cell II	767 ± 50	11.7 ± 2.5	63 ± 5	5.6 ± 0.8
Cell III	990 ± 50	19.3 ± 2.5	74 ± 5	14.2 ± 1.0

Figure 5: (a) Representative light J-V curves measured under AM 1.5 global 1-sun illumination. (b) External Quantum Efficiency (EQE) for InAlAs solar cells with different window layers. Bottom: table containing a summary of the figures of merit for the different InAlAs solar cells. Cell I: $\text{In}_{0.47}\text{Al}_{0.53}\text{As}$ window, cell II: $\text{In}_{0.35}\text{Al}_{0.65}\text{As}$ window, cell III: $\text{In}_{0.35}\text{Al}_{0.65}\text{As}$ window + $\text{In}_{0.53}\text{Ga}_{0.47}\text{As}$ cap layer.

REFERENCES

- [1] M. A. Green, K. Emery, Y. Hishikawa and W. Warta. "Solar cell efficiency tables (version 37)" *Prog. Photovolt: Res. Appl.* **19**, 2011, pp. 84-92.
- [2] J. F. Geisz, D. J. Friedman, J. S. Ward, A. Duda, W. J. Olavarria, T. E. Moriarty, J. T. Kiehl, M. J. Romero, A. G. Norman, and K. M. Jones. "40.8% efficient inverted triple-junction solar cell with two independently metamorphic junctions" *Appl. Phys. Lett.* **93**, 2008, 123505 1-3.
- [3] R. R. King. "Multijunction cells Record breakers" *Nature Photonics.* **2**, 2008, pp. 284-286.
- [4] Y. Takeda, M. Wakai, T. Ikeoku, and A. Sasaki. "InAlAs/InGaAs low-band-gap cell on InP for high efficiency multi-structure solar cell system". *Sol. Energy Mater. Sol. Cells.* **26**, 1992, pp. 99-103.
- [5] M. S. Leite, R. L. Woo, W. D. Hong, D. C. Law, and H. A. Atwater. "Wide-band-gap InAlAs solar cell for an alternative multijunction approach". *Appl. Phys. Lett.* **98**, 2011, pp. 093502 1-3.

ACKNOWLEDGMENTS

The authors acknowledge financial support from the Department of Energy - Solar Energy Technologies Program under Grant No. DE-FG36-08GO18071. This work benefited from use of the Caltech Kavli Nanoscience Institute and the Material Science TEM facilities partially supported by the MRSEC Program of the National Science Foundation under Award Number DMR-0520565.